HHS Public Access

Author manuscript

J Aerosol Sci. Author manuscript; available in PMC 2016 January 13.

Published in final edited form as:

J Aerosol Sci. 2014 September ; 75: 65–80. doi:10.1016/j.jaerosci.2014.04.008.

Influence of secondary aspiration on human aspiration efficiency

K.R. Anderson and **T. Renee Anthony**

Department of Occupational and Environmental Health, University of Iowa, 105 River Street, Iowa City, IA 52242, USA

Abstract

Computational fluid dynamics (CFD) was used to evaluate the contribution of secondary aspiration to human aspiration efficiency estimates using a humanoid model with realistic facial features. This study applied coefficient of restitution (CoR) values for working-aged human facial skin to the facial regions on the humanoid CFD model. Aspiration efficiencies for particles ranging from 7 to 116 μm were estimated for bounce (allowing for secondary aspiration) and no-bounce (CoR=0) simulations. Fluid simulations used the standard k–epsilon turbulence model over a range of test conditions: three freestream velocities, two breathing modes (mouth and nose breathing, using constant inhalation), three breathing velocities, and five orientations relative to the oncoming wind. Laminar particle trajectory simulations were used to examine inhaled particle transport and estimate aspiration efficiencies. Aspiration efficiency for the realistic CoR simulations, for both mouth- and nose-breathing, decreased with increasing particle size, with aspiration around 50% for 116 μm particles. For the CoR=0 simulations, aspiration decreased more rapidly with increasing particle size and approached zero for 116 μm compared to realistic CoR models (differences ranged from 0% to 80% over the particle sizes and velocity conditions). Differences in aspiration efficiency were larger with increasing particle size (>52 μm) and increased with decreasing freestream velocity and decreasing breathing rate. Secondary aspiration was more important when the humanoid faced the wind, but these contributions to overall aspiration estimates decreased as the humanoid rotated through 90°. There were minimal differences in aspiration between uniform CoR values of 0.5, 0.8, 1.0 and realistic regionally-applied CoR values, indicating differences between mannequin surfaces and between mannequin and human skin will have negligible effect on aspiration for facing-the-wind orientation.

Keywords

Computational fluid dynamics; Human aspiration efficiency; Coefficient of restitution; Particle bounce; Inhalability

1. Introduction

The focus of occupational measurement of aerosols is to evaluate worker exposure to aerosols. Thus sampling methods should reflect a biologically relevant measurement. Particles are not inhaled with 100% efficiency, especially as particle size increases. The human head can be thought of as an aerosol sampler and the faction of particles that enters the head is a function of the breathing rate, freestream velocity, and head dimensions. The

different sampling conventions (inhalable, respirable, and thoracic) reflect this size-selectiveness of the human respiratory system. Inhalable particles are described as those that have the ability to penetrate the plane of the nose/mouth.

Early inhalability studies (Ogden and Birkett, 1975, Armbruster and Breuer, 1982 and Vincent and Mark, 1982) investigated human aspiration using mannequins as human surrogates in wind tunnel studies. In these studies, an inhaling mannequin was placed in a uniform concentration of particles and the mass concentration inhaled through the nose or mouth by the mannequin was measured. The concentration inhaled by the mannequin is divided by the concentration in the freestream to give estimates of aspiration. This process is repeated over a range of particle sizes to define aspiration as a function of particle size. The studies by Ogden and Birkett (1975), Armbruster and Breuer (1982) and Vincent and Mark (1982), summarized by Soderholm (1989), formed the basis for the ACGIH inhalability particulate mass (IPM) criterion, given by

$$\mathrm{IPM}=0.5\left(1+\exp\left(-0.06\mathrm{d_a}\right)\right)\mathrm{IPM}=0.5\left(1+\exp\left(-0.06\mathrm{da}\right)\right) \quad (1)$$

where d_a is the aerodynamic diameter (μm) of particles being sampled and defines the desired collection efficiency of inhalable aerosol samplers. Examining human aspiration efficiency has relied on wind tunnel experiments, such as the ones described above, or computational fluid dynamics.

When particles directly enter the mouth/nose it is called primary aspiration. When particles bounce first on a surface (the face or exterior sampler walls) and then are entrained in the airflow before entering the mouth/nose it is called secondary aspiration. If experimental studies use mannequins as surrogates for humans, then there is an underlying assumption is that particles will interact with mannequin surface the same as for human facial skin, which may not be an appropriate assumption given skin and plastics may differ in elasticity.

When a particle strikes a surface with sufficient energy to overcome adhesion to the object, the particle bounces off a surface and becomes resuspended in air rather than depositing on the surface. When the critical velocity, V_{cr}, of the particle is exceeded, particles will bounce or rebound on a surface (Wu et al., 2006). The critical velocity depends on many factors, including the particle size, the mechanical properties of the particle and surface, the adhesion/surface energy, and surface roughness.

The coefficient of restitution (CoR) is defined as the ratio of the rebound velocity to the impacting velocity during a collision between two objects. In aerosol science, the value is related to characteristics of both the surface material and the particle striking that surface. A CoR of 1.0 represents a perfectly elastic collision, where 100% of the velocity at impact is retained by the colliding particle, whereas a CoR of 0 represents an inelastic collision, where the particle retains zero velocity upon impact and, therefore, does not bounce.

The mechanisms of particle rebound on solid surfaces have been well described in the literature (Brach et al., 2000, Dahneke, 1971, Dahneke, 1972 and Dahneke, 1995; Konstandopoulos and Rosner, 1997 and Konstandopoulos, 2006; among others). For example, Dahneke (1973) investigated the sticking probability of latex spheres striking

polished quartz and stainless steel and Kim and Dunn (2008) examined glass spheres dropped on a silica target plate. While aerosol samplers are made out of materials similar to those used in these studies, the flat surfaces used in these idealistic cases cannot account for particle interaction with more complex geometries, such as those in aerosol samplers.

In addition to mechanistic studies of rebounding particles, other studies have focused on characterizing particle bounce on and into aerosol samplers in order to reduce sampling errors (Ingham and Yan, 1994 and Vincent and Gibson, 1981). Secondary aspiration resulting from particle bounce, blow-off, roll-off, and re-entrainment has been considered for both thick-walled, disk shaped inlets (Belyaev and Levin, 1972, Belyaev and Levin, 1974 and Vincent and Gibson, 1981) and for thin-walled, sharp edged inlets (Lipatov et al., 1986, Lipatov et al., 1988 and Grinshpun et al., 1993). Vincent and Gibson (1981) found particle bounce increased aspiration when particle size increased and when the ratio of sampling velocity to ambient wind speeds increased. They reported that bouncing particles can significantly contribute to the particle mass collected by three blunt shaped disk samplers with a range of inlet diameters (2, 3, and 4 mm). Mark et al. (1982) found particle bounce was a function of wind speed and was more pronounced for larger (40 μm) particle sizes and decreased with decreasing particle size using Casella type T13032 dust samplers with the exterior surface of the sampler clean and greased.

While studies are available examining particle bounce on metallic surfaces, both flat surfaces and more complex samplers, limited work has been done to evaluate bounce on human skin. While idealistic mechanistic studies and sampler studies are useful for theoretical development of particle rebound equations and reducing sampling errors, these studies are not always applicable to understanding secondary aspiration associated with particles bouncing off the facing and becoming aspirated into the mouth/nose of a breathing human because of differences in both shape and surface characteristics. Human facial features result in a complex surface shape, with protrusions and rounded edges that differ from flat plates or samplers with relatively simple geometries. An understanding of the CoR for particles impacting the human skin is necessary to investigate particle transport following impaction on facial skin. Human facial skin has been shown to be non-uniform, with CoRs for the cheeks, forehead and nose having significantly different values, with regional average CoRs of 0.74, 0.55 and 0.61, respectively (Anderson et al., 2014). Although significant differences were identified between participant age category, gender and season of the year (winter and summer), differences in CoR were in the range of 0.05, which may be negligible for aerosol research of human aspiration.

Understanding how particles bounce off of facial features is critical to understanding and quantifying the human aspiration efficiency of particles, particularly if secondary aspiration results from particles impacting the face. Computer models can incorporate the complex surface of the human head, where the angle of the incident particle can be accurately simulated. However, simulations require an estimate of the CoR to determine how much energy results in a particle rebound versus deposition. Previous computational studies have been conducted investigating the effect of orientation on human oral (Anthony & Anderson, 2013) and nasal aspiration (Anderson & Anthony, 2014), the effect of torso complexity on aspiration (Anderson & Anthony, 2013) using similar geometries. The computational

models used a humanoid geometry with realistic facial features but a simplified, truncated torso. Anthony & Anderson (2013) found that trends in aspiration efficiency agreed with those found in experimental wind tunnel studies. Good agreement was found with the linear inhalable particulate mass equation proposed by Aitken et al. (1999) at 0.1 m s^{-1} freestream velocities. Anderson and Anthony (2014) expanded on the previous CFD study to investigate nasal inhalation. They found the same trends as for the mouth-breathing simulations, namely aspiration decreased with increasing particle size. Furthermore they found that there appeared to be an upper size limit for aspiration efficiency for nose-breathing around 100 μm. Anderson and Anthony (2013) investigated the effect of torso complexity on aspiration efficiency and found that while increasing torso complexity changes the location where particles are inhaled, aspiration efficiency changed by less than 10%. As the focus of the previous work was on effects of orientation and torso geometry, the previous studies assumed a CoR of 0, ignoring the effect of particle bounce, and thus secondary aspiration. This study uses similar geometry used in the previous studies but while the dimensions are the same, the head is divided into six distinct regions in order to evaluate the effect of CoR on human aspiration efficiency estimates. Anthony and Flynn (2006) examined a humanoid geometry but did not explicitly evaluate particle bounce. They investigated particles with trajectories towards the mouth and found that while including “towards the mouth” estimates improved agreement with Kennedy and Hinds (2002) experimental wind tunnel results, the simulations overestimated aspiration for particles in the middle portion of the aspiration curve, indicating that bounce differences may be important. Other modelers investigating human inhalability (King Se et al., 2010) have only modeled primary aspiration (CoR=0) and ignored the effects of particle bounce. While wind tunnel sampler studies have tried to eliminate bounce by greasing surfaces of the sampler, wind tunnel inhalability studies using mannequins have not reported controlled for particle bounce (Ogden & Birkett, 1975; Aitken et al.,1999; Kennedy and Hinds, 2002 and Sleeth and Vincent, 2011).

Differences between experimental inhalability research studies might be a result of different mannequin surfaces used as the human surrogate to study inhalability. Results from human aspiration efficiency studies have shown aspiration efficiencies to decrease with increasing particle size, to a greater extent than earlier experimental work indicated. One potential reason for this discrepancy could be the effect of particle bounce in experimental mannequin studies (Aitken et al.,1999; Kennedy and Hinds, 2002 and Sleeth and Vincent, 2011), leading to larger estimates of aspiration efficiency. Experimental studies use a wide range of test aerosols and mannequins (Table 1) made out of different materials which would have different CoR values. For example, Kennedy and Hinds (2002) used a fiberglass mannequin coated with conductive paint, whereas Aitken et al. (1999) used a resuscitation mannequin (Little Anne model) constructed of lightweight plastic with latex skin stretched over the face. Although both used similar test aerosols (aluminum oxide spheres), the surface of these mannequins would have different CoRs, which could lead to differences in secondary aspiration owing to different particle interactions at the face of the mannequins. If experimental studies are accounting for secondary aspiration and computation studies are not allowing particle bounce on the surface (Anthony & Anderson, 2013; King Se et al., 2010) then comparisons between results may not be valid.

It is important to know whether particle rebound contributes significantly to human aspiration measurements so samplers can be developed to match a physiologically relevant measure of exposure. Assuming particles deposit and do not bounce could result in an *underestimation* of aspiration efficiencies in conditions where particles have the potential to bounce on the face and be re-entrained into the airstream to be inhaled. However, using unrealistically high CoR values (hard plastic versus human skin) could potentially overestimate human aspiration. To accurately model secondary aspiration and determine appropriate values for experimental mannequins, it is important to understand the sensitivity of aspiration efficiency to CoR value, and whether uniform CoR values are sufficient or if more precise (regional CoR) values are necessary.

The objectives of this study were to determine whether secondary aspiration significantly increases human aspiration efficiency estimates, using generic and realistic values of CoR for human mouth and nose breathing. An evaluation of the complexity of CoR assignment (region versus uniform, whole-face) will be made for the facing-the-wind orientation, along with an estimate of between-mannequin aspiration differences that may be attributable to changes in inhalable mannequin surface materials from wind tunnel study tests.

2. Methods

Computational fluid dynamics was used to solve the fluid flow around a simulated inhaling mannequin and to solve particle trajectories to calculate aspiration efficiency into an inhaling mannequin. Ansys Software (Design Modeler, Meshing Application and Fluent 12.1 and 13.0, Ansys Lebanon, NH, USA) was used for geometry creation, mesh generation and fluid simulations. Once the fluid simulations were solved, particle trajectories were simulated to determine the upstream area where particles are inhaled and subsequent calculation of aspiration.

Table 2 identifies the simulation variables examined in this study. Three freestream velocities were investigated: 0.1, 0.2, 0.4 m s^{-1}, which represent a range of indoor velocities typical of occupational settings (Baldwin & Maynard, 1998). Two modes of inhalation were examined: mouth and nose-breathing, both represented as continuous inhalation. For mouth-breathing simulations, breathing velocities of 1.81, 4.33, and 12.11 m s^{-1} were applied to the mouth surface, which represent at-rest, moderate and heavy breathing, respectively. Nose-breathing simulations used velocities of 2.49 and 5.96 m s^{-1}, representing at-rest and moderate breathing at the nostril surface. The velocities applied were selected to be mathematically equivalent to the mean inhalation velocity of sinusoidal breathing at 7.5, 20.8 and 50.3 L min^{-1} for the at-rest, moderate and heavy breathing.

2.1. Geometry

As shown in Fig. 1, a realistic human head, with a small nose, small lip facial geometry, was evaluated in this work, described fully in Anthony (2010). The mouth was modeled as a rectangular opening with rounded edges (area=1.385e^{-4} m^2) and the nostrils were modeled as ovals located 2.4 mm above the bottom plane of the nose (area=1.00614e^{-4} m^2). The center of the mouth was positioned at the origin (0, 0, 0). The torso height was set at 1.23 m, which represented a torso truncated at hip height. For computational studies relying on a

uniform concentration in the freestream, a truncated torso is a reasonable simplification for aspirational efficiency estimates (Anderson & Anthony, 2013). For facing-the-wind orientation, lateral symmetry was assumed, allowing for only half of the computational domain to be simulated, thereby reducing computational time. For the other orientations, both sides of the humanoid and a full-width wind tunnel were modeled, as the assumption of lateral symmetry was not appropriate. The computational domain around the forms was positioned to simulate a wind tunnel. Figure 2 illustrates the location of the humanoid geometry in the simulated wind tunnel. For all facial geometries, the center of the mouth was located at the origin, with the inlet wall placed 1.85 m in front and the outlet wall 1.80 m behind the mouth center. The height and width of the domain were 1.23 m and 1.14 m, respectively, with the center of the mouth located 0.87 m below the ceiling of the wind tunnel. The dimensions of the domain ensured that the flow was fully developed upstream of the torso, no acceleration occurred through the outflow of the domain and that the location of the walls did not influence the fluid field. The humanoid model was rotated through five discrete orientations to the oncoming wind: 0 (facing-the-wind), 15°, 30°, 60°, 90°. This procedure allowed for the evaluation of secondary aspiration on the forward-facing aspiration efficiency estimate, where it was anticipated secondary aspiration would have the most impact. As the model rotates past 90°, particles would be more likely to impact on the back of the head, thus bounce would be less of a concern for these orientations.

2.2. Mesh generation and refinement

Ansys 13.0 was used to mesh the computational domain (Ansys Inc., Lebanon, NH, USA). A paved meshing scheme, which uses triangular surfaces and tetrahedral volumetric elements, was applied to the volume within the simulated wind tunnel.

The most refined mesh from previous simulations was applied to the model (Anthony & Anderson, 2013), which had approximately 3 million nodes throughout the domain. Previous studies (Anthony and Anderson, 2013 and Anderson and Anthony, 2014) have documented solutions solved using this mesh density to be well converged and be independent of the mesh. The average node spacing throughout the domain was 17 mm, and the average spacing around the mouth was more refined (0.477 mm) to better characterize flow near the head.

2.3. Computational method

Simulations were conducted on 64-bit processor personal computers with 8–12 gigabytes RAM using Windows XP and Windows 7 operating systems. The steady-state, incompressible, turbulent Navier–Stokes equations were solved using Fluent 12.1 and 13.0 (Ansys Inc., Lebanon, NH, USA). Uniform inlet velocities were applied to both the wind tunnel entrance and mouth or nostril openings, per values in Table 2. The wind tunnel exit was assigned as an outflow, which enforced no acceleration through the surface but computed the velocities on the surface to assure continuity. A plane of symmetry was assigned to the “floor” of the wind tunnel, which allowed flow along but not through the surface. All other surfaces in the domain were assigned the no-slip condition (“wall”), where velocity and turbulence parameters were set to zero. All other unassigned nodes were assigned initial velocities equivalent to the freestream velocity (0.1, 0.2 or 0.4 m s^{-1}),

according to the simulation underway. For all tests, an 8% turbulent intensity and a ratio of eddy to laminar viscosity of 10, typical of wind tunnel studies, were assigned to the domain entrance as a boundary condition and as initial conditions to all unassigned nodes throughout the domain.

The standard k–epsilon turbulence model was used to simulate turbulent flow, using the enhanced wall function. Full buoyancy effects were modeled. Gravity was set to act downward at 9.81 m s^{-2}. Indoor room air temperature was simulated (20 °C) with the corresponding air density (1.205 kg m^{-3}) and viscosity (1.83692×10^{-5} kg m^{-1} s^{-1}).

Solutions were obtained using the SIMPLE algorithm, with second order upwinding, when the global solution errors (GSE) reached predetermined tolerances of 10^{-5}. Previous studies have shown that solutions are changing less than 2% for orientations 0–60° and less than 5% for 90° between GSE tolerances of 10^{-4} and 10^{-5}.

2.4. Bounce simulations

Once fluid simulations were completed, facial features were assigned the CoR values to allow particles to rebound from the facial surfaces and examine their effect on aspiration efficiency estimates. A subset of simulations, for facing-the-wind orientation, mouth-breathing, investigated the sensitivity of aspiration efficiency to regionally versus uniformly applied CoR values. First, constant values were applied to the entire face, including the top and back of the head (0.0, 0.5, 0.8, 1.0). Next, CoR values were applied to specific facial regions (Table 3) corresponding to mean values provided by Anderson et al. (2014) for forward-facing orientations (0–90°). CoRs set at constant coefficients of 0.55, 0.61, and 0.74 were assigned to the forehead, nose, and cheek, respectively. In all cases, the normal and tangential coefficients of restitution were set to the same value. For the CoR=0 simulations (no-bounce condition), any particle that contacted any surface was modeled as deposited. For other settings, any particle that struck the face was assigned a post-contact velocity equivalent to CoR×initial velocity, with the travel angle equal to the impact angle×CoR. As such, the CoR=0 condition represents the expected minimum aspiration efficiency, whereas the regionally-averaged CoR simulations reflects a more realistic aspiration. When particles contacted all other solid surfaces in the domain, including the top and back of head and temporal region, they were assumed to deposit.

2.5. Particle release and tracking

Particles were released and tracked as described in previous studies (Anthony & Anderson, 2013). In brief, once the quality of the fluid field estimates were evaluated, particle simulations were conducted to identify critical areas, the area enclosing all particle release locations with trajectories that terminate in the mouth/nose, which were used to estimate aspiration efficiencies for each geometry and velocity condition. The Eulerian–Lagrangian approach was used to solve for particle motion. Laminar particle trajectories were examined: thus, the estimates of aspiration efficiency reflect mean values and cannot incorporate uncertainty due to turbulent particle behavior. Particle momentum equations and spherical drag law are described fully in Supplemental A. The spherical drag law was used to compute the drag coefficient (Morsi & Alexander, 1972). Particle simulations used a 50-μm length

scale, which determined the maximum distance the particle will travel before the particle trajectory was updated. To control the error when calculating the pathlines, the tolerance was set at $1e^{-6}$. The maximum refinement or the largest number of step size refinements in one single integration step was set to 20 step sizes. Sensitivity tests were conducted to ensure aspiration did not change with decreasing length scale, increasing tolerance or maximum refinement settings.

For each set of simulation conditions, particle trajectories of seven particle sizes were examined (7, 22, 52, 68, 82, 100, and 116 μm). These particle sizes were chosen to match experimental data from Kennedy and Hinds (2002) and simulations of Anthony and Anderson (2013).

Non-evaporating, unit density spheres were released, which allowed for reporting in aerodynamic diameters. The release points were located more than four head diameters away from the torso models to ensure that the freestream was not affected by the downstream bluff-body (Chung & Dunn-Rankin, 1997). As such, the particles were released 0.75 m upstream of the mouth opening for particles smaller than 82 μm. Particles 82 μm and larger were released closer to the torso (X=0.4 m upstream of the mouth opening) to take into account the effect of gravitational settling and to allow for the particles to be released at locations below the boundary layer at the top of the computational domain to minimize wall effects. For these particles, release positions were sufficiently upstream and above the head so that bluff body effects in this region were negligible (no bluff-body velocity reduction from torso blockage, no increased velocity from acceleration over the head, and no lateral or vertical turning to go around the head, confirmed for each condition). For freestream velocity of 0.1 m s^{-1}, gravitational settling of the particle required closer release locations (X=0.2 m upstream, for the particle sizes 100 and 116 μm); we again confirmed that velocities at these release locations differed from the freestream velocity by less than 1%.

To meet the uniform particle distribution assumption, particles were released at velocities that incorporated the freestream velocity at that location and at the particle's terminal settling velocity (Table 2). This was accomplished by assigning a horizontal velocity equal to the velocity in the wind tunnel at the release position and a vertical velocity equal to the combination of the initial velocity of the freestream at the release location combined with a downward component equal to the terminal settling velocity of the particle being evaluated.

2.6. Determination of critical area

Particle simulations were performed to identify the upstream positions and cross-sectional area where particles would travel through the freestream and terminate in the mouth, thereby being inhaled, defined as the critical area. These positions were identified by stepping through a series of lateral (Y) positions (ΔY=0.0005 m) and releasing 100 particles along a 10 mm vertical line (ΔZ=0.0001 m) to determine the position of the minimum and maximum particle that would be inhaled at a given lateral position. The critical area was computed, as detailed in Anthony and Flynn (2006). The number of particles inhaled was multiplied by the z interval between particles (0.0001 m), which was multiplied by the interval between the lateral positions (0.0005 m). Across a series of Y coordinates, a set of heights (Z coordinates) defined the location of the critical area.

2.7. Aspiration efficiency calculation

Once the critical area was identified for each test condition, the aspiration efficiency fraction was computed using:

$$A=\frac{A_{critical}U_{critical}}{A_{mouth}U_{mouth}} \quad (2)$$

where $A_{critical}$ is the upstream critical area, A_{mouth} is the mouth opening, $U_{critical}$ is the upstream freestream velocity, and U_{mouth} is the inhalation velocity. Orientation-averaged aspiration was computed for each velocity condition and particle size by weighing the five individual estimates by the orientation's average contribution to the 180° (±90°) rotation:

$$A=\frac{1}{12}A_0+\frac{1}{6}A_{15}+\frac{1}{4}A_{30}+\frac{1}{3}A_{60}+\frac{1}{6}A_{90} \quad (3)$$

where the subscripts refer to the orientation relative to the oncoming wind and the weighing factor represents the proportion of the complete rotation that the study angle covers, similar to Tsai et al.(1995). For each particle size (7), velocity condition (6), CoR (5) and breathing mode (2), critical areas and aspiration estimates were computed.

2.8. Data analysis

Coordinates of critical areas were plotted to examine differences between CoR simulations. Forward (±90°) orientation-averaged aspiration efficiencies by freestream and inhalation velocity were computed for both mouth and nose-breathing simulations. For each particle size, aspiration efficiency was averaged over all freestream and breathing velocities to provide mean orientation-averaged aspiration efficiencies. Differences between simulations, both single orientation and orientation-averaged, were computed to evaluate contribution of particle rebound to estimates of aspiration efficiency.

3. Results

3.1. Fluid simulations

Simulations required up to five days to reach solution levels at 10^{-5} GSE. The heavy breathing conditions required more time to solve and required more iterations to achieve convergence to the 10^{-5} global tolerance. Pressure was usually the last degree of freedom to reach the specified GSE level. Fluid flows were simulated for 75 unique fluid flow models (three freestream velocities, mouth-breathing geometry at three breathing rates, nose-breathing geometry at two breathing rates, and five orientations). L2 and R_2 error norms were evaluated for one velocity condition (0.2 m s freestream and moderate, mouth-breathing) to confirm convergence (Supplementary material).

3.2. Critical areas and particle trajectories

Illustrations of particle trajectory simulations are presented in Fig. 3. Illustrations are shown for the 15° orientation, at 0.2 m s^{-1} freestream and moderate breathing rate. As displayed, smaller particles (Figs. 3a and b, 4a and b) tended to approach the face following the streamlines mostly horizontal with a slight upward path consistent with air approaching a

bluff body. When secondary aspiration occurred for the smaller particles and CoR>0 (Figs. 3b and 4b), particles impacted on the nose and cheeks prior to being inhaled. The larger particles (Figs. 3d and 4d) had a more vertical trajectory component, consistent with settling velocities exceeding freestream velocities; these secondary aspirations were from particles impacting on the forehead prior to being inhaled. These trends were consistent across all breathing velocities and freestream velocities.

Representative plots of critical areas for 7 and 100 μm particles at 0.2 m s^{-1} freestreams and moderate mouth-breathing are given in Fig. 5 and Fig. 6, respectively. Critical areas were calculated for each particle size, mode of breathing, orientation, and bounce simulation. Critical areas for the realistic, regionally-averaged CoR simulations were on average 71% larger compared to the CoR=0 simulations. Differences in critical areas between CoR increased with decreasing freestream velocity, indicating that bounce plays a more important role in aspiration in slower moving air. The upper and lower edge of the critical areas increased with realistic CoR values for particles >52 μm owing to particles bouncing on the forehead and lips, as illustrated in Fig. 3. Critical areas for particles <52 μm were similar in size and shape, as these particle sizes were less affected by particle bounce. While the edges of the critical areas increased vertically, the critical area was not observed to substantially increase horizontally. Small particles bounced off the cheeks and once re-entrained in the airflow followed air streamlines past the mannequin's face. Large particles that bounced off the cheeks continued downwards due to gravitational settling, or bounced away from the mouth and nose.

3.3. Aspiration efficiency estimates

3.3.1. Mouth-breathing simulations—Figure 7 illustrates the orientation averaged aspiration efficiencies for the regionally-averaged CoRs for each velocity condition for forward-facing orientations (0–90°) and mouth-breathing simulations. Aspiration was highest for small particles and decreased with increasing particle size for both CoR simulations. Aspiration was highest at the facing-the-wind orientation and decreased with increasing rotation away from the centerline for both the realistic CoR and CoR=0. Table 4 presents the differences in aspiration efficiency between realistic CoRs and CoR=0 for each test condition and mode of breathing. For mouth-breathing simulations, aspiration efficiency decreased with increasing particle size, but less so with realistic CoR compared to CoR=0 simulations. For CoR=0, aspiration for at-rest breathing simulations resulted in no particles 100 μm or larger being inhaled, regardless of freestream velocity or orientation (Anthony & Anderson, 2013). This situation was due to particles being blocked by and terminating on the nose. For this work, however, only particles ≥100 μm for the at-rest mouth-breathing condition at the 90° orientation were not inhaled. Forward-facing aspiration efficiency remained higher for particle sizes ≥82 μm when compared to the CoR=0 simulations for larger particles (around 50%).

Allowing for secondary aspiration resulted in higher aspiration efficiencies compared to the CoR=0 models. Differences were small for particles <68 μm, on average 3%. For particles ≥68 μm, differences were on average 27%. Over all test conditions and particle sizes, differences in aspiration between the realistic CoR and CoR=0 ranged from 0% to 80%.

Comparisons in aspiration efficiency for a uniform (0.5, 0.8 and 1.0) and regional CoRs were made for the mouth-breathing simulations at the 0.2 and 0.4 m s^{-1} freestream velocities for the at-rest and heavy breathing rates only at facing-the-wind orientation. No meaningful differences in aspiration between realistic CoR and uniform CoRs of 0.5, 0.8, and 1.0 were identified. Differences in aspiration efficiency between the realistic, regionally-applied CoRs and a uniform CoR of 1.0 were relatively small (on average 5%).

3.3.2. Nose-breathing simulations—Table 4 presents the differences in aspiration efficiencies between realistic CoR and CoR=0 simulations for nose-breathing inhalation for all test conditions. As shown in Fig. 8, differences in aspiration efficiency between the realistic CoR and CoR=0 simulations increased for particle diameters ≥52 μm. Similar to the mouth-breathing simulations, allowing for secondary aspiration resulted in higher aspiration efficiencies compared to the CoR=0 simulations for the nose-breathing models. On average over all test conditions, differences between the CoR simulations were small (2.2%) for particles <52 μm. For particle sizes ≥52 μm differences between realistic CoR and CoR=0 simulations were on average 40% and ranged from 0% to 70%. These differences more substantial at the 0.1 m s^{-1} freestream velocity, compared to differences at 0.2 and 0.4 m s^{-1} freestream velocities, which would indicate that secondary aspiration is more important at lower freestream velocities where gravitational settling causes particles to bounce off a surface and settle downwards, whereas at higher freestream velocities particles were more likely to strike a surface and bounce away from the nose and avoid aspiration. Differences in aspiration efficiency for the realistic CoR simulations between nose and mouth-breathing inhalation were small. Mouth-breathing aspiration efficiencies were on average 2% higher (maximum 5%) compared to the nose breathing aspiration efficiencies for the realistic CoR simulations. For the CoR=0 simulations, differences between the mouth breathing and nose breathing were more noticeable (on average 11%, maximum 21%).

4. Discussion

Allowing for particle bounce on the humanoid facial features in CFD simulations increased the critical area, resulting in significantly higher estimates of aspiration efficiency. This study showed that for the forward-facing orientation, particle bounce was more important for particles ≥68 μm than for smaller particles, where particle bounce increased aspiration efficiencies by only 3%.

While the shape of the critical area is informative and important for aspiration calculation, the position of the critical area is not relevant due to truncation simplification of the model. Anderson and Anthony (2013) found truncating the humanoid model affects the location of the critical area, but not the size or shape. Critical areas decreased with increasing particle size, similar to results from previous studies (Anthony, 2010, Anthony and Anderson, 2013 and King Se et al., 2010). As the humanoid model rotated away from the facing-the-wind orientation, critical areas decreased, as anticipated (Kennedy & Hinds, 2002).

Anderson et al. (2014) reported the CoR measured on study participants varies regionally across the face. The effect of uniform versus regional CoR values was evaluated in this work and differences in aspiration efficiency estimates were minimal (5%). This finding is

important for both modelers and experimental work because it indicates that an average uniformly applied CoR to the surface of the mannequin or inhaling humanoid model is an appropriate simplification when evaluating human aspiration efficiency. This finding would also indicate that the use of mannequins, with constant CoR values, would be reasonably good surrogates for human facial skin.

Anderson et al. (2014) reported an average CoR of 0.68 for a resuscitation mannequin made of hard plastic with standard latex (2.46 mm thick) stretched over the face (Little Anne model) and hypothesized that this mannequin type (Resusci Anne, Laerdal, Stavanger, Norway) may be a good human surrogate for experimental wind tunnel work, if uniform CoR values are sufficient for evaluating aspiration estimates. It was hypothesized that there would be no significant differences in aspiration efficiency between uniformly applied CoR values of 0.5, 0.8 and 1.0. The results from this study support that hypothesis. Although CoRs for fiberglass mannequins and mannequins made of hard plastics are anticipated to have values higher than the resuscitation mannequin with a latex face mask, their CoR values are within the 0.5–1.0 range investigated in this study. As no meaningful differences in aspiration were found with CoR values ranging from 0.5 to 1.0, differences in mannequins between experimental studies would not have a significant effect on inhalability studies, another important finding for experimental wind tunnel studies. The application of any CoR larger than 0.5 resulted in significantly higher aspiration compared to the simulations with CoR=0 indicating that it is necessary to report whether particle bounce on the surface of the mannequin was controlled for, which many experimental studies do not currently do.

Anderson et al. (2014) also found significant differences in CoR by gender and season (winter versus summer), although those differences were in the range of 0.05, but hypothesized those small changes in CoR may not be physically relevant for aerosol work. No significant differences in aspiration between simulations with changes as large as 0.3 in CoRs were found, supporting this hypothesis that changes in CoR of 0.05 would have negligible effect on inhalability studies. Furthermore, this finding would indicate that the slight changes in CoR due to different solid test particles between experiments may not have a meaningful effect on aspiration efficiency, if they are within the range investigated here (0.5–1.0).

Aspiration estimates were compared to published data in the literature. Figure 9 compares facing-the-wind mouth-breathing aspiration efficiency for the realistic CoR and CoR=0 simulations at the 0.4 m s^{-1} freestream and moderate breathing velocity to published experimental data from Kennedy and Hinds (2002). Previous work reported good agreement for particles up to 52 μm, but lower aspiration for larger particle sizes (Anthony & Flynn, 2006). The authors hypothesized that the differences in aspiration for particles >52 μm could be due to particle bounce, different breathing patterns (Kennedy & Hinds (2002) investigated cyclic breathing and peak inhalation was higher than the simulated constant 4.33 m s^{-1} inhalation investigated), differences in head and mouth dimensions, and turbulent particle transport (simulations only evaluated laminar particle transport). Allowing for secondary aspiration in the model results in aspiration curves similar in shape to the curve reported by Kennedy and Hinds (2002) but the simulated curve still had 30% higher

aspiration efficiencies for 82 and 116 μm particles. The aspiration efficiency curves for both the realistic CoR and Kennedy and Hinds (2002) data show aspiration decreasing as particle size increases to 52 μm, but then increasing for 68 and 82 μm before decreasing again. The increase in aspiration at 68 μm was due to particles bouncing off the forehead and nose, then being inhaled. As particle size increases past 68 μm, gravitational settling makes it more difficult for particles to be inhaled, hence the decrease with increasing particle size. Particles <68 μm bounced on the nose and lips but their horizontal trajectories caused them to bounce away from the inhaling mouth.

Aspiration efficiency estimates were compared to the IPM and Aitken et al.'s (1999) proposed low velocity criteria. Aspiration efficiency estimates for the realistic CoR simulations were higher compared to the IPM criterion but there was good agreement between the realistic aspiration efficiency curves and the proposed low velocity criterion. The simulated aspiration efficiency curves are for forward-facing (±90°) orientations only and the IPM criterion is for orientation-averaged over 360°. Not including the rear-facing orientations would cause aspiration efficiency estimates to be slightly higher compared to full orientation-averaged estimates. Orientation with the back towards the wind is anticipated to reduce aspiration efficiency, and better agreement over the full 360° rotation may be found.

In an effort to explain differences in results between inhalability studies, other research has been conducted to assess the sensitivity of aspiration to factors including: facial feature dimensions, breathing velocity, freestream velocity, torso simplifications, turbulence modeling, wall functions, and body heat of the mannequin. Anthony (2010) reported differences in facial features affecting aspiration by 10% and differences in breathing velocity affecting aspiration on average 21%. Anderson and Anthony (2013) reported simplifications in torso geometry affecting aspiration by 9%. Differences in turbulence models (standard k–epsilon and realizable) and wall function affect aspiration on average by 2% (range 0–14%) and <1%, respectively. Sleeth and Vincent (2011) investigated the effect of body heat in experimental studies and did not find changes in airflow patterns around an inhaling mannequin, although the effect on aspiration was not explicitly evaluated. Aitken et al. (1999) also did not find significant differences in aspiration between experimental studies using a mannequin heated and unheated. Our study shows on average 5% difference in aspiration between uniform CoRs ranging from 0.5 to 1.0. The 5% difference in aspiration due to differences in CoRs combined with the 10% difference in aspiration owing to differences in facial feature dimensions and 2% from different turbulence models can account for 17% of the variability between results, which would bring simulated results much closer to experimental results by Kennedy and Hinds (2002). What has not yet been thoroughly investigated to date is the effect of turbulent particle tracking schemes, which could account for some of the remaining differences between simulated and experimental results. Accounting for secondary aspiration in the CFD model brings simulated results closer in agreement to experimental results.

While this study presents improvements in aspiration simulation models, several limitations to this study remain. The first is the use of steady inhalation as a simplification of cyclical breathing. Exhalation has been shown to affect airflow patterns around the mouth and could

have an influence on aspiration efficiency. Future work should consider whether the same findings hold with cyclical breathing. Further, the humanoid model was only rotated through forward-facing orientations (±90°). Rotation was limited to forward-facing orientations because it was anticipated that particle bounce would have the largest effect at these orientations. As the human geometry rotates past 90° (side to the wind), particles have been seen to impact on the back of the head, where we expect particles to get trapped in the hair; hence, bounce is less of a concern for these orientations and differences in particle bounce on the face were anticipated to be minimal.

The particle simulations did not allow particles to interact or bounce on each other, whereas in an experimental setup this bouncing could occur and cause particle agglomeration. Particles impacting on a surface would either all bounce at the specified CoR or “deposit” and be removed from the simulation. Probability of particles sticking was not assessed in the model, which is a simplification from reality, where some particles may stick while others bounce. If some particles stick while others bounce then modeled aspiration that assumes all particles bounce would cause aspiration efficiency estimates to be higher. The method used for particle simulation to obtain the critical areas does not reflect actual concentrations but rather simulated aspiration of an infinite concentration of particles released in the upstream air to locate the position of the critical areas. Although this study identified the upstream locations where particles are aspirated, future work could conduct additional simulations using a separate method to release realistic concentrations to investigate particle collision and agglomeration associated with particles bouncing on the face.

Skin oils and moisture would also play an important role in particle dynamics, along with facial hair and skin pore size. Although these factors were ignored in the model, particles that were secondarily aspirated were those that bounced on the forehead, nose tip, and lips. Particles 52 μm and smaller bounced on the nose and lips, while particles larger than 52 μm bounced on the forehead and cheeks due to the vertical trajectory component from gravitational settling. Facial hair, such as moustaches or beards probably might not reduce secondary aspiration, due to the locations where particle bounce occurred. Large particles that bounced off the chin bounced downwards due to gravitational settling, thus large particles would not be aspirated even if not trapped by a beard. Small particles bounced on the chin bounced away from the mouth/nose following airstreams. There was very little difference in aspiration between simulations with CoR≠0 and CoR=0 for 7 and 22 μm particles, which were the most likely to bounce off the upper lip which would most likely to be influenced by a moustache. Due to the vertical trajectory of large particles, the nose tip projected far enough in front of the upper lip that large particles were not able to reach the upper lip to bounce in, thus moustaches would also minimally impact secondary aspiration. Increased skin oil or moisture would most likely occur on the forehead, which would increase particle deposition and decrease secondary aspiration for the larger particles due to the “stickier” surface of the skin. Bangs or hair covering the forehead would also decrease secondary aspiration for larger particles because they would trap particles rather than allow them to bounce. The effect of skin oil and hair on the forehead would have less of an effect on secondary aspiration for smaller particles as they are less likely to bounce in those locations.

5. Conclusion

This study showed that the selection of different formulations of the coefficient of restitution in computation models of human aspiration can have an important effect, and that ignoring bounce entirely could result in a significant *underestimation* of aspiration efficiency, particularly in the facing-the-wind orientation and freestream velocities <0.1 m s^{-1}. Larger particle sizes increase differences in aspiration efficiency estimates more than smaller particle sizes, where differences are less than 5%. Negligible differences in aspiration estimates were observed between realistic-regionally applied CoR values and uniform CoR values, indicating a single CoR value is acceptable for modeling and experimental purposes. Furthermore, aspiration was relatively insensitive to the CoR value ranging from 0.5 to 1.0 for forward-facing orientations, thus differences in mannequin surfaces in that range would not have a meaningful impact on inhalability studies. The differences in results between experimental and computational studies can be attributed, in part, to the effect of particle bounce on the surface of the mannequin. If between-study comparisons are to be made, it is important to report the type of aerosol (solid versus liquid) and whether secondary aspiration was allowed or if the surface of the mannequin was treated to prevent particle bounce.

Supplementary Material

Refer to Web version on PubMed Central for supplementary material.

References

Aitken RJ, Baldwin PEJ, Beaumont GC, Kenny LC, Maynard AD. Aerosol inhalability in low air movement environments. Journal of Aerosol Science. 1999; 30(5):613–626.

Anderson KR, Anthony TR. Uncertainty in aspiration efficiency estimates from torso simplifications in computational fluid dynamics simulations. Annals of Occupational Hygiene. 2013; 57(2):184–199. [PubMed: 23006817]

Renée Anthony T, Renée Anderson K. Computational fluid dynamics investigation of human aspiration in low-velocity air: orientation effects on mouth-breathing simulations. Annals of Occupational Hygiene. 2013:740–757. [PubMed: 23316076]

Anderson KR, Anthony TR. Computational fluid dynamics investigation of human aspiration in low velocity air: orientation effects on nose-breathing simulations. Annals of Occupational Hygiene. 2014

Anderson KR, Oleson JJ, Anthony TR. Variability in coefficient of restitution in human facial skin. Skin Res Technol. 2014

Anthony TR, Flynn MR. Computational fluid dynamics investigation of particle inhalability. Journal of Aerosol Science. 2006; 37(6):750–765.

Anthony TR. Contribution of facial feature dimensions and velocity parameters on particle inhalability. Annals of Occupational Hygiene. 2010; 54(6):710–725. [PubMed: 20457783]

Armbruster L, Breuer H. Investigations into defining inhalable dust. Annals of Occupational Hygiene. 1982; 26(1):21–32. [PubMed: 7181266]

Baldwin PE, Maynard AD. A survey of wind speeds in indoor workplaces. Annals of Occupational Hygiene. 1998; 42(5):303–313. [PubMed: 9729918]

Belyaev SP, Levin LM. Investigation of aerosol aspiration by photographing particle tracks under flash illumination. Journal of Aerosol Science. 1972; 3(2):127–140.

Belyaev SP, Levin LM. Techniques for collection of representative aerosol samples. Journal of Aerosol Science. 1974; 5(4):325–338.

Brach RM, Dunn PF, Li X. Experiments and engineering models of microparticle impact and deposition. The Journal of Adhesion. 2000; 74(1–4):227–282.

Chung I, Dunn-Rankin D. Experimental investigation of air flow around blunt aerosol samplers. Journal of Aerosol Science. 1997; 28(2):289–305.

Dahneke B. The capture of aerosol particles by surfaces. Journal of Colloid and Interface Science. 1971; 37(2):342–353.

Dahneke B. The influence of flattening on the adhesion of particles. Journal of Colloid and Interface Science. 1972; 40(1):1–13.

Dahneke B. Measurements of bouncing of small latex spheres. Journal of Colloid and Interface Science. 1973; 45(3):584–590.

Dahneke B. Particle bounce or capture—search for an adequate theory: I. conservation-of-energy model for a simple collision process. Aerosol sci technol. 1995; 23.1:25–39.

Grinshpun S, Willeke K, Kalatoor S. A general equation for aerosol aspiration by thin-walled sampling probes in calm and moving air. Atmospheric Environment: Part A General Topics. 1993; 27(9): 1459–1470.

Ingham DB, Yan B. Re-entrainment of particles on the outer wall of a cylindrical blunt sampler. Journal of Aerosol Science. 1994; 25(2):327–340.

Kennedy NJ, Hinds WC. Inhalability of large solid particles. Journal of Aerosol Science. 2002; 33(2): 237–255.

Kim OV, Dunn PF. Direct visualization and model validation of microsphere impact and surface capture. J Aerosol Sci. 2008; 39.4:373–375.

King Se CM, Inthavong K, Tu J. Inhalability of micron particles through the nose and mouth. Inhalation Toxicology. 2010; 22(4):287–300. [PubMed: 20070173]

Konstandopoulos AG, Rosner DE. The initial sticking fraction of inertially impacting particles on cylindrical and spherical collectors. Journal of Aerosol Science. 1997; 28:S89–S90.

Konstandopoulos AG. Particle sticking/rebound criteria at oblique impact. Journal of Aerosol Science. 2006; 37(3):292–305.

Lipatov GN, Grinshpun SA, Semenyuk TI, Sutugin AG. Secondary aspiration of aerosol particles into thin-walled nozzles facing the wind. Atmospheric Environment (1967). 1988; 22(8):1721–1727.

Lipatov GN, Grinspun SA, Shingaryov GL, Sutugin AG. Aspiration of coarse aerosol by a thin-walled sampler. Journal of Aerosol Science. 1986; 17(5):763–769.

Mark DJHWA, Vincent JH, Witherspoon WA. Particle blow-off: a source of error in blunt dust samplers. Aerosol Science and Technology. 1982; 1(4):463–469.

Morsi SA, Alexander AJ. An investigation of particle trajectories in two-phase flow systems. Journal of Fluid Mechanics. 1972; 55(2):193–208.

Ogden TL, Birkett JL. The human head as a dust sampler. Inhaled Particles. 1975; 4:93–105. [PubMed: 1236176]

Ogden TL, Birkett JL. An inhalable-dust sampler, for measuring the hazard from total airborne particulate. Ann Occup Hyg. 1978; 21.1:41–50. [PubMed: 655531]

Sleeth DK, Vincent JH. Proposed modification to the inhalable aerosol convention applicable to realistic workplace wind speeds. Annals of Occupational Hygiene. 2011; 55(5):476–484. [PubMed: 21257744]

Soderholm SC. Proposed international conventions for particle size-selective sampling. Annals of Occupational Hygiene. 1989; 33(3):301–320. [PubMed: 2802448]

Tsai P-J, et al. Impaction model for the aspiration efficiencies of aerosol samplers in moving air under orientation-averaged conditions. Aerosol science and technology. 1995; 22.3:271–286.

Vincent JH, Gibson H. Sampling errors in blunt dust samplers arising from external wall loss effects. Atmospheric Environment (1967). 1981; 15(5):703–712.

Vincent JH, Mark D. Applications of blunt sampler theory to the definition and measurement of inhalable dust. Annals of Occupational Hygiene. 1982; 26(1):3–19. [PubMed: 7181272]

Wu J, Fang H, Yoon S, Kim H, Lee C. The rebound phenomenon in kinetic spraying deposition. Scripta Materialia. 2006; 54(4):665–669.

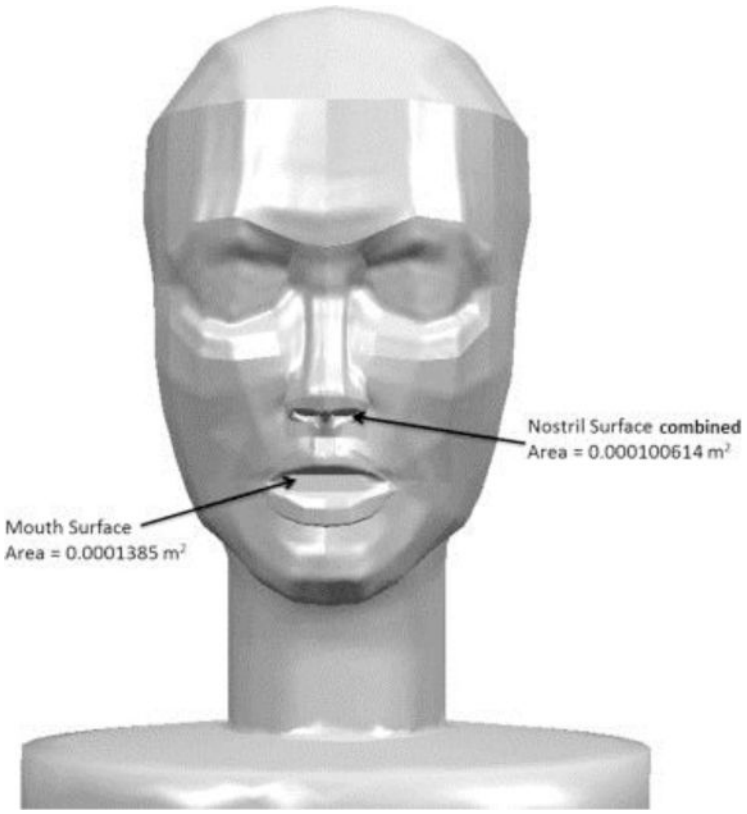

Fig. 1.

Simulation facial geometries. Areas of both mouth and nose geometries are given. Inhalation occurred either through the nose or mouth for a given simulation.

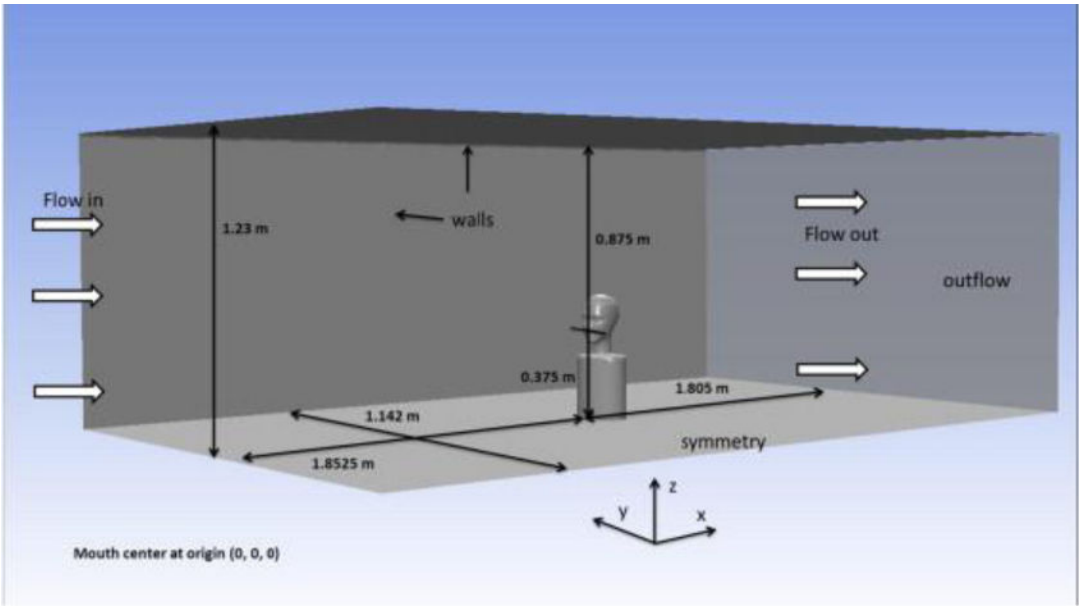

Fig. 2.

Computational domain example for a humanoid at 0° to the oncoming wind (facing-the-wind). Large white arrows indicate direction of the flow, set at 0.1, 0.2, or 0.4 m s^{-1}, depending on the simulation underway. Origin is positioned at the center of the mouth.

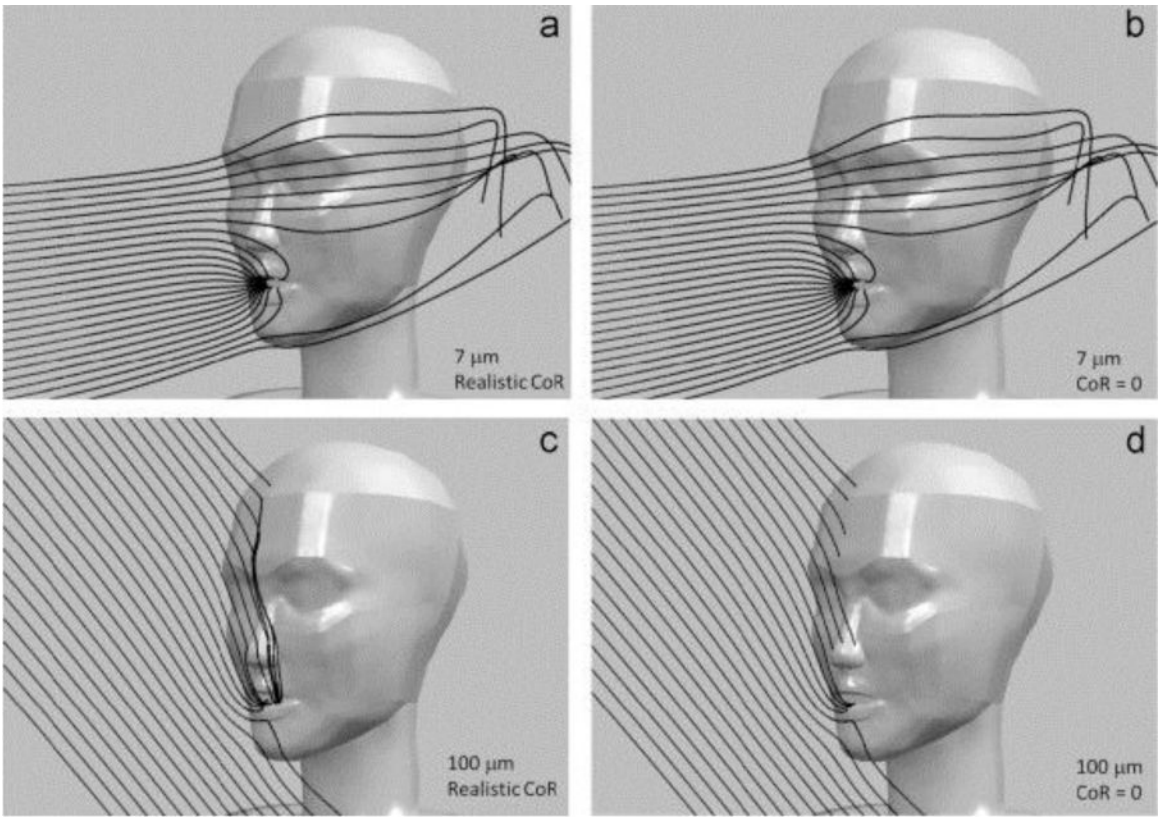

Fig. 3.

7 µm (a and b) and 100 µm (c and d) particle trajectories for 0.2 m s^{-1} freestream velocity and moderate, mouth breathing inhalation at 15° orientation. Each image shows 25 particles released upstream at 0.01 m to the right of the mouth center (*Y*) over a vertical distance of 0.13 m (*Z*). Realistic CoR simulations are on left. CoR=0 simulations are on right.

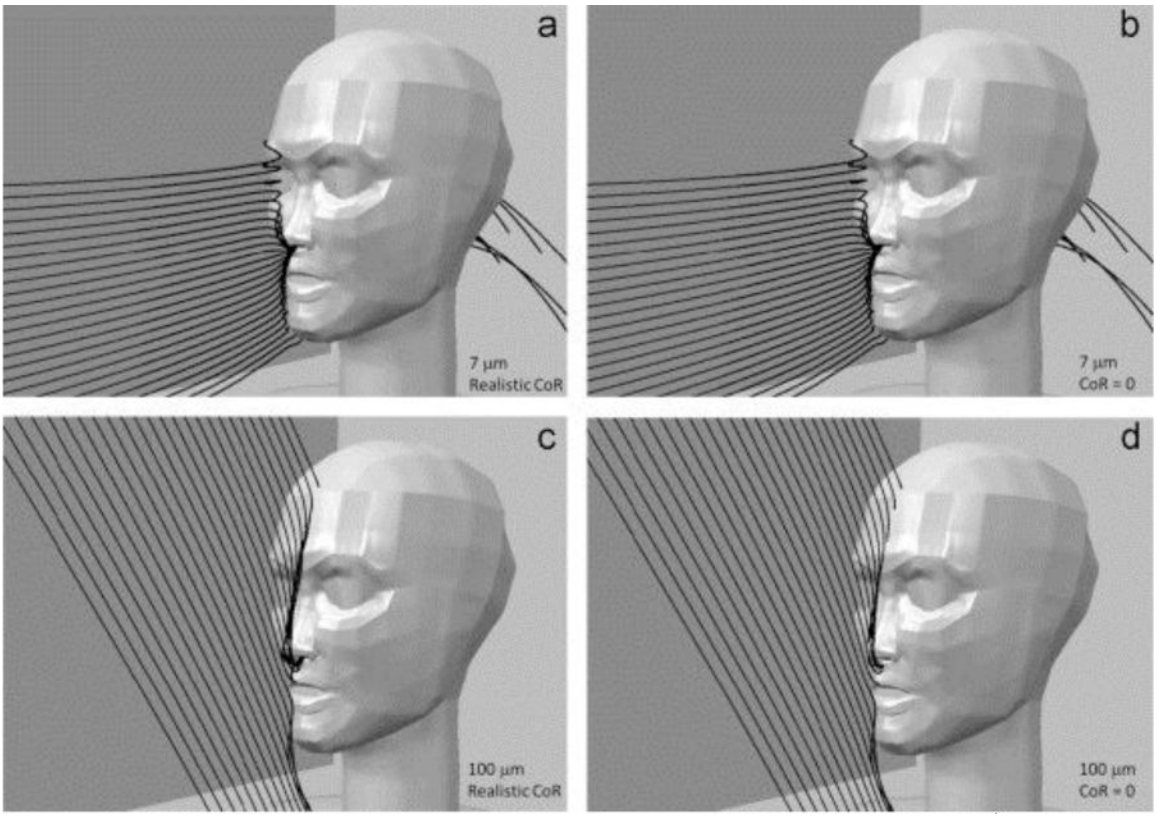

Fig. 4.

7 µm (a and b) and 100 µm (c and d) particle trajectories for 0.2 m s^{-1} freestream velocity and moderate, nose breathing inhalation at 15° orientation. Each image shows 25 particles released upstream at 0.01 m to the right of the mouth center (*Y*) over a vertical distance of 0.13 m (*Z*). Realistic CoR simulations are on left. CoR=0 simulations are on right.

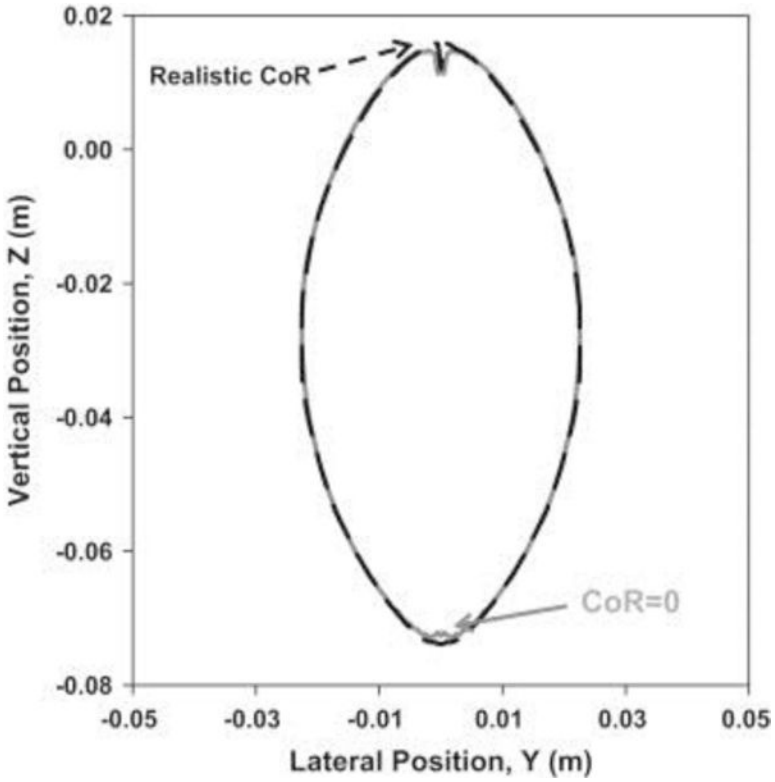

Fig. 5.

Comparison of critical areas for realistic CoR and CoR=0 for 7 μm particles at 0.2 m s^{-1} freestream velocity, moderate mouth-breathing inhalation. The black dashed line represents realistic CoR simulation and the gray line represent CoR=0 simulations.

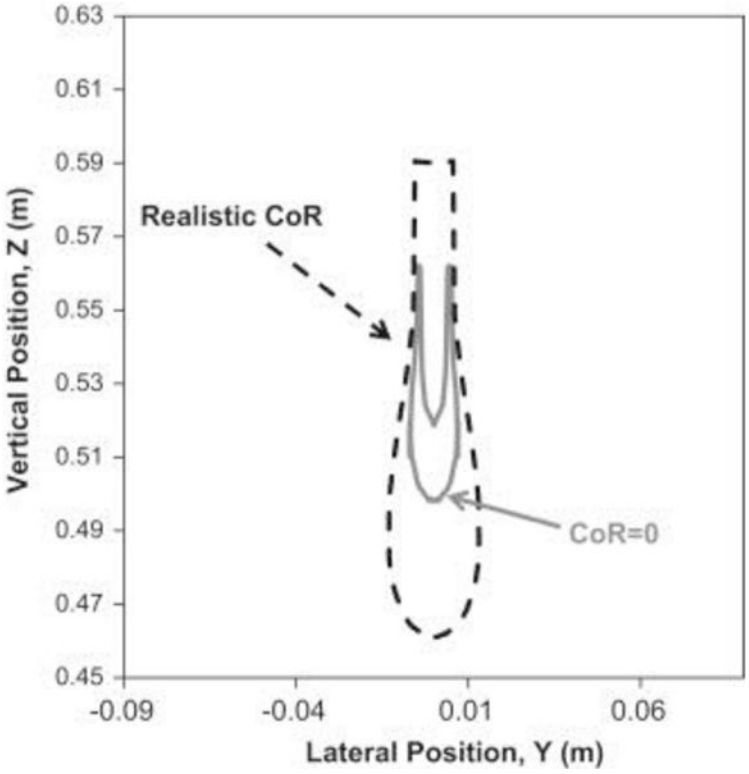

Fig. 6.

Comparison of critical areas for realistic CoR and CoR=0 for 7 μm particles at 0.2 m s^{-1} freestream velocity, moderate mouth-breathing inhalation. The black line represents realistic CoR simulations and gray lines represents CoR=0 simulations.

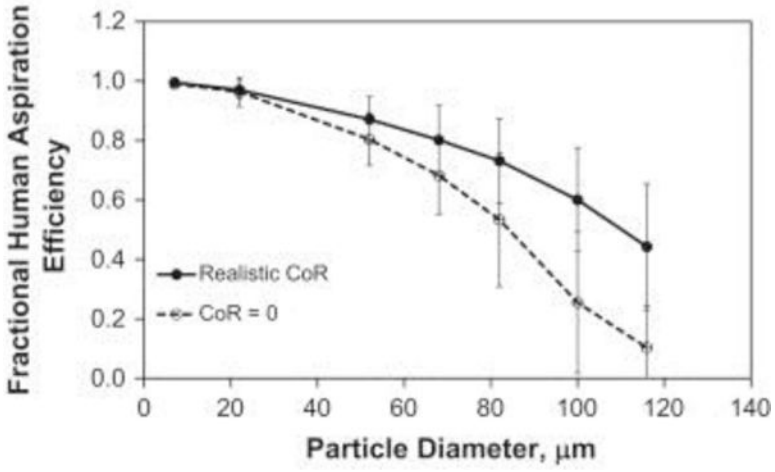

Fig. 7.

Comparison of orientation-averaged aspiration (fraction) for averaged over all simulation conditions for the realistic CoR simulations and CoR=0 simulations for mouth-breathing inhalation. The solid lines represent simulations with realistic CoR and the dashed lines represent CoR=0 simulations. Orientation-averaged over forward-facing orientations (0–90°). Standard deviations represent variability between velocity conditions.

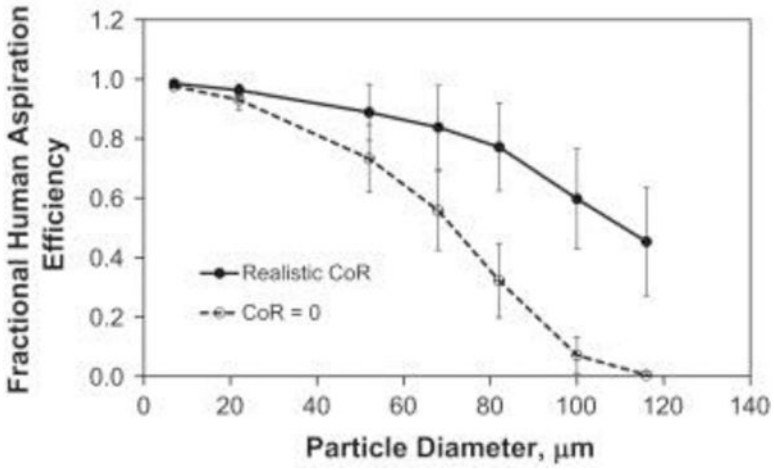

Fig. 8.

Comparison of orientation-averaged aspiration (fraction) for averaged over all simulation conditions for the realistic CoR simulations and CoR=0 simulations for nose-breathing inhalation. The solid lines represent simulations with realistic CoR and the dashed lines represent CoR=0 simulations. Orientation-averaged over forward-facing orientations (0–90°). Standard deviations represent variability between velocity conditions.

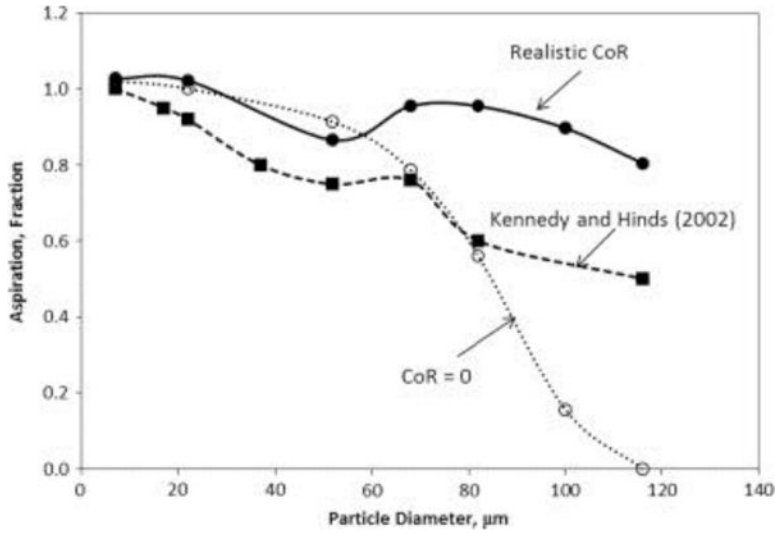

Fig. 9.

Simulation aspiration efficiency for facing-the-wind orientation at 0.4 m s^{-1} freestream velocity, moderate mouth-breathing compared to experimental facing-the-wind mouth-breathing aspiration data from Kennedy and Hinds (2002).

J Aerosol Sci. Author manuscript; available in PMC 2016 January 13.

Table 1

Summary of experimental inhalability setup.

Authors	Freestream velocity	Inhalation	Orientation	Test aerosol		Size range	Mannequin	Controlled for bounce
Odgen and Birkett (1977)	0.75, 2.75 m/s	84, 1340 ml/s	Rotated discrete, stepwise 45° angles to on-coming wind	Bis(2-ethylhexyl)sebacate, tagged with fluorescent dye	Liquid	Up to 30 μm	Human head, shoulders, and chest	Not reported
		(5, 80.4 Lpm)						
Ogden and Birkett (1978)	Calm air	5, 20, 40 Lpm	Stationary	Liquid fluorescent monodisperse particles	Liquid	Up to 30 μm	Human head, shoulders, and chest	Not reported
Armbruster and Breuer (1982)	0.3–8 m/s	10.8, 20.0, and 37.5 Lpm	Discrete angles 0°, 90°, 180°	Coal dust	Solid	Up to 100 μm	Mannequin head only	Not reported
Vincent and Mark (1982)	1, 2, and 4 m/s	20 Lpm	Facing-the-wind	Aluminum oxide	Solid	10–100 μm	Human head mounted on full-sized torso, truncated at knee height	Not reported
Aitken et al. (1999)	Calm air	6, 10, 20 Lpm	Stationary	Near monodisperse fused alumina	Solid	6–90 μm	Full-sized mannequin, restitution mannequin constructed of lightweight plastic with latex skin over face	Not reported
Hsu and Swift (1999)	Calm air	8.5 and 20 Lpm	Stationary	Narrowly graded aluminum oxide powders	Solid	13–135 μm	Head, upper torso	Not reported
Kennedy and Hinds (2002)	0.4, 1, 1.6 m/s	14.2, 20.8, and 37.3 Lpm	One full rotation per sampling run	Narrowly graded aluminum oxide powders	Solid	7–116 μm	Full-sized, full torso fiberglass mannequin, coated with conductive paint and grounded	Not reported
Sleeth and Vincent (2011)	0.1, 0.2, and 0.4 m/s	6, 20 Lpm	360° one direction, 360° opposite direction, reciprocal pattern through sampling run	Narrowly graded powders of fused alumina	Solid	6–90 μm	Full-sized truncated at waist height mannequin	Not reported

Table 2

Simulation variables investigated in study. *N* indicates the number of conditions.

Parameter	**Settings**	***N***
Geometry	Small nose, small lips	1
Breathing mode	Mouth-breathing	2
	Nose-breathing	
Freestream velocity	0.1, 0.2, 0.4	3
Inhalation velocity (m s^{-1})	Mouth-breathing: 1.81, 4.33, 12.11	3
	Nose-breathing: 2.49, 5.96	2
Orientation (deg)	0, 15, 30, 60, 90	5
Particle aerodynamic diameter (mm)	7, 22, 52, 68, 82, 100, 116	7
Associated terminal settling velocity (m s^{-1})	1.47e−3, 0.0146, 0.0813, 0.1391, 0.2023, 0.3008, 0.4048	–

Table 3

CoR values applied to surfaces on humanoid. CoRs were applied as constant coefficients. Normal and tangential CoRs were set to the same value.

Region	CoR
Cheeks	0.74
Eye, forehead	0.55
Mouth	0.74
Nose, philtrum	0.61
Top, back of head, neck, remaining torso	0

Table 4

Difference in aspiration efficiency (percentage) between realistic CoR and CoR=0 simulations, mouth-breathing and nose-breathing simulations.

Mode of inhalation	Particle size (μm)	Mouth breathing		Nose breathing	
Simulation condition		Facing-the-wind	Orientation-averaged	Facing-the-wind	Orientation-averaged
0.1 m s^{-1} Freestream velocity, at-rest breathing	7	–	–	1	1
	22	–	–	2	2
	52	–	–	21	19
	68	–	–	38	38
	82	–	–	61	60
	100	–	–	69	61
	116	–	–	53	42
0.1 m s^{-1} Freestream velocity, moderate breathing	7	1	0	1	0
	22	1	0	10	3
	52	7	7	14	28
	68	13	14	29	27
	82	19	22	53	46
	100	67	63	72	71
	116	62	57	66	68
0.1 m s^{-1} Freestream velocity, heavy breathing	7	1	0	–	–
	22	0	−2	–	–
	52	4	5	–	–
	68	6	9	–	–
	82	10	14	–	–
	100	13	19	–	–
	116	42	42	–	–
0.2 m s^{-1} Freestream velocity, at-rest breathing	7	1	1	1	1
	22	1	1	2	2
	52	12	11	20	14
	68	32	19	37	26
	82	67	36	62	41
	100	78	38	80	39
	116	0	8	61	24

J Aerosol Sci. Author manuscript; available in PMC 2016 January 13.

Mode of inhalation	Particle size (μm)	Mouth breathing		Nose breathing	
Simulation condition		Facing-the-wind	Orientation-averaged	Facing-the-wind	Orientation-averaged
0.2 m s^{-1} Freestream velocity, moderate breathing	7	1	1	1	1
	22	1	1	3	2
	52	5	7	14	11
	68	11	12	30	22
	82	25	18	54	39
	100	66	45	80	62
	116	68	44	78	64
0.2 m s^{-1} Freestream velocity, heavy breathing	7	1	1	–	–
	22	1	1	–	–
	52	5	6	–	–
	68	8	10	–	–
	82	10	14	–	–
	100	32	25	–	–
	116	42	37	–	–
0.4 m s^{-1} Freestream, at-rest breathing	7	2	0	0	2
	22	2	1	2	7
	52	8	6	21	32
	68	24	11	45	28
	82	49	26	72	41
	100	70	34	100	39
	116	37	20	83	27
0.4 m s^{-1} Freestream velocity, moderate breathing	7	1	1	1	1
	22	2	1	1	3
	52	5	6	17	17
	68	17	11	39	27
	82	39	15	60	44
	100	74	33	83	46
	116	80	39	90	44
0.4 m s^{-1} Freestream velocity, heavy breathing	7	1	1	–	–
	22	1	1	–	–

J Aerosol Sci. Author manuscript; available in PMC 2016 January 13.

Mode of inhalation	Particle size (μm)	Mouth breathing		Nose breathing	
Simulation condition		Facing-the-wind	Orientation-averaged	Facing-the-wind	Orientation-averaged
	52	4	6	–	–
	68	10	10	–	–
	82	22	13	–	–
	100	34	20	–	–
	116	39	26	–	–